

# Modelling the nonlinear shear stress-strain response of glass fibre-reinforced composites. Part II: Model development and finite element simulations

W. Van Paepegem<sup>\*</sup>, I. De Baere and J. Degrieck

Ghent University, Dept. of Mechanical Construction and Production,  
Sint-Pietersnieuwstraat 41, 9000 Gent, Belgium

## Abstract

The ASTM D3518/D3518M-94(2001) Standard Test Method for "*In-Plane Shear Response of Polymer Matrix Composite Materials by Tensile Test of a  $\pm 45^\circ$  Laminate*" is based on the uniaxial tensile stress-strain response of a  $\pm 45^\circ$  composite laminate which is symmetrically laminated about the midplane. For long glass fibre-reinforced epoxy composites, the test shows a highly nonlinear shear stress-strain curve. This work is concerned with the development of a material model to predict this mechanical behaviour. Part I discusses the experimental program with tensile tests on  $[+45^\circ/-45^\circ]_{2s}$  laminates and off-axis  $[10^\circ]_8$  composites. Cyclic tensile tests have been performed to assess the amount of permanent shear strain and the residual shear modulus.

Part II focuses on the development of the material model and the finite element implementation. Two state variables have been introduced to represent the shear modulus degradation and the accumulation of permanent shear strain. The model has also been applied to the simulation of a three-point bending test on a  $[+45^\circ/-45^\circ]_{2s}$  laminate.

**Keywords** A: Polymer-matrix composites (PMCs); B: Mechanical properties; C: Damage mechanics; D: Mechanical testing.

## 1. Introduction

In Part I [1], the experimental results for the static tensile tests on  $[+45^\circ/-45^\circ]_{2s}$  laminates and off-axis  $[10^\circ]_8$  composites have been discussed, together with the cyclic tensile tests on  $[+45^\circ/-45^\circ]_{2s}$  specimens. It appeared that both shear modulus degradation and accumulation of permanent shear strain are important factors contributing to the resulting nonlinear shear stress-strain curve.

In literature, several modelling approaches can be distinguished. Some of them are based on the micromechanical approach, where a representative volume element is built up with three phases: the fibres, the matrix and the fibre/matrix interface [2-4]. With these models, the effect of a damaged bonding interface can be assessed. On the other hand, the mesomechanical models start from the ply level and develop relations between the homogenized lamina stresses and strains. Ladevèze and Le Dantec [5] use the Continuum Damage Mechanics theory for describing matrix microcracking and fibre/matrix debonding. In order to model the anelastic strains induced by damage, a plasticity model has been

---

<sup>\*</sup> Corresponding author (Fax: +32-(0)9-264.35.87, E-mail: Wim.VanPaepegem@UGent.be).

applied. Payan and Hochard [6] have adopted the approach by Ladevèze and Le Dantec to study the static and fatigue behaviour of  $[\pm 45^\circ]_{3s}$  carbon/epoxy laminates.

Lafarie-Frenot and Touchard [7] have conducted a large experimental study on the inplane shear behaviour of long carbon-fibre composites with thermoset and thermoplastic matrix. They found a marked decrease in secant shear modulus values associated with the development of large plastic strains.

In this paper, the Continuum Damage Mechanics theory constitutes the framework for the mesomechanical model. Two state variables are introduced: the shear damage  $D_{12}$  and the permanent shear strain  $\gamma_{12}^p$ . In the next paragraph, their evolution laws are developed, based on a phenomenological approach.

## 2. Development of the model

With the definitions of shear damage  $D_{12}$  and permanent shear strain  $\gamma_{12}^p$  (see Part I [1], Figure 14), the evolution of these variables in function of the total shear strain  $\gamma_{12}$  is plotted in Figure 1 and Figure 2 respectively for the three cyclic  $[\pm 45^\circ/-45^\circ]_{2s}$  tensile tests IH6, IG4 and IH2.

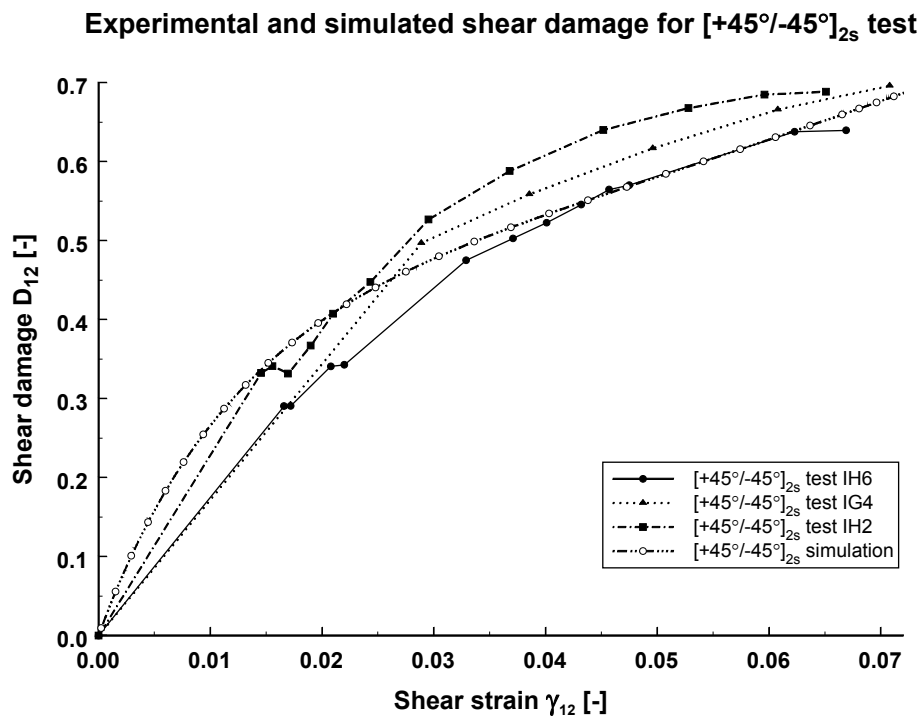


**Figure 1** Evolution of the shear damage  $D_{12}$  for three cyclic  $[\pm 45^\circ/-45^\circ]_{2s}$  tensile tests.

### Experimental and simulated permanent shear strain for $[+45^\circ/-45^\circ]_{2s}$ test

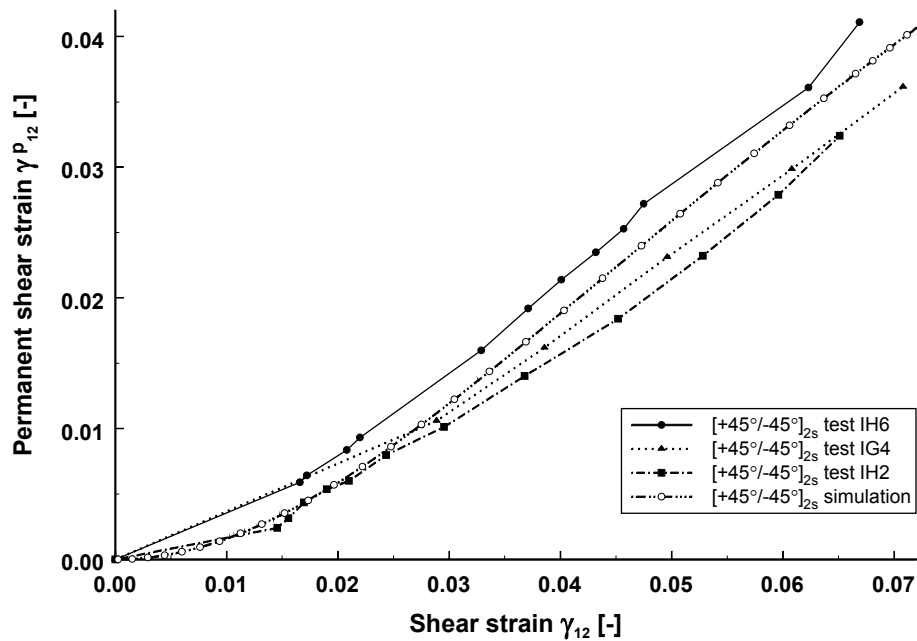


Figure 2 Evolution of the permanent shear strain  $\gamma_{12}^p$  for three cyclic  $[+45^\circ/-45^\circ]_{2s}$  tensile tests.

Several assumptions have been made to establish the models for the shear damage  $D_{12}$  and permanent shear strain  $\gamma_{12}^p$ :

- both damage variables show an exponential behaviour,
- the value of both variables must be monotonically increasing,
- the shear modulus degradation should depend on the elastic part  $\gamma_{12}^e = \gamma_{12} - \gamma_{12}^p$  of the total shear strain  $\gamma_{12}$ ,
- the accumulation of permanent shear strain  $\gamma_{12}^p$  is assumed to depend on the total shear strain  $\gamma_{12}$ .

On the basis of these equations, the following phenomenological model has been put forward:

$$\begin{aligned} \frac{dD_{12}}{d\gamma_{12}^e} &= c_1 \cdot \exp(c_2 \cdot D_{12}) \\ \frac{d\gamma_{12}^p}{d\gamma_{12}} &= c_3 \cdot \gamma_{12} \cdot \exp(c_4 \cdot \gamma_{12}^p) \end{aligned} \quad (1)$$

where  $c_1, \dots, c_4$  are material constants. The material constants have been optimized, based on the experimental data of Figure 1 and Figure 2. Their values are listed in Table 1.

Table 1 Material constants.

$c_1$	39.0
-------	------

$c_2$	-1.55
$c_3$	32.0
$c_4$	-32.0

With these values of the material constants, the simulated results are shown in Figure 1 and Figure 2 for the evolution of the shear damage  $D_{12}$  and permanent shear strain  $\gamma_{12}^p$  respectively.

Of course, the model should be capable of simulating the corresponding shear stress-strain curves of the static  $[+45^\circ/-45^\circ]_{2s}$  tensile tests IH3, IG2 and IH4, as the loading history has no significant effect on the damage evolution. Figure 3 shows the experimental and simulated results. So, based on the prediction of the shear modulus degradation and the accumulation of the permanent shear strain, the resulting shear stress – shear strain curve can be simulated.

**Experimental and simulated shear stress-strain curves for  $[+45^\circ/-45^\circ]_{2s}$  tests**

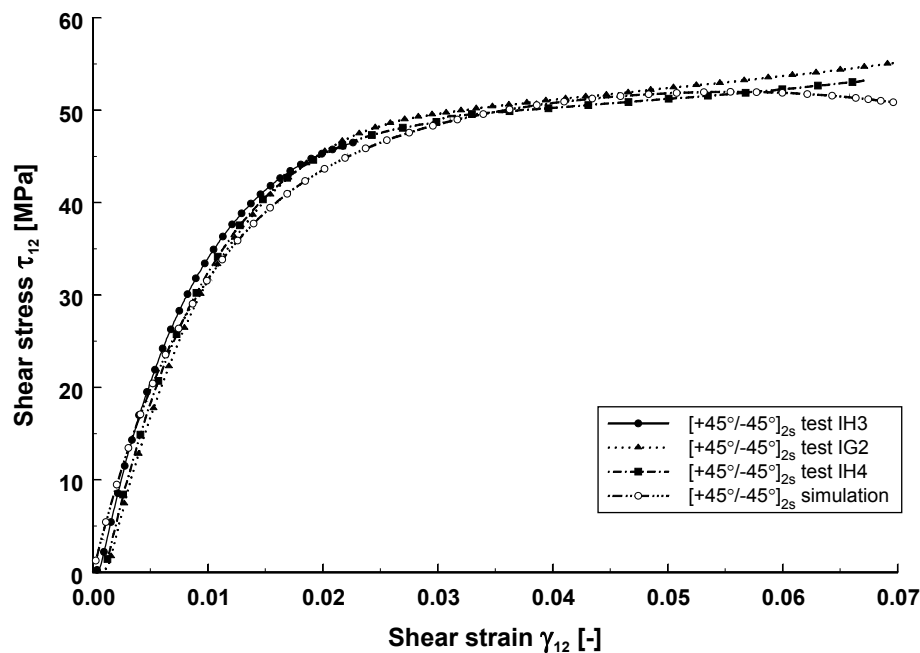


**Figure 3** Experimental and simulated shear stress-strain curve for the static  $[+45^\circ/-45^\circ]_{2s}$  tensile tests IH3, IG2 and IH4.

If the different shear modulus  $G_{12}^0$  of the  $[10^\circ]_8$  off-axis specimens is taken into account (see Part I [1]), the model is also capable of predicting the shear stress-strain response of the static  $[10^\circ]_8$  tensile tests IC3 and IC4, with the same values for the four material constants  $c_1, \dots, c_4$ . This is illustrated in Figure 4.

### Experimental and simulated shear stress-strain curves for $[10^\circ]_8$ tests

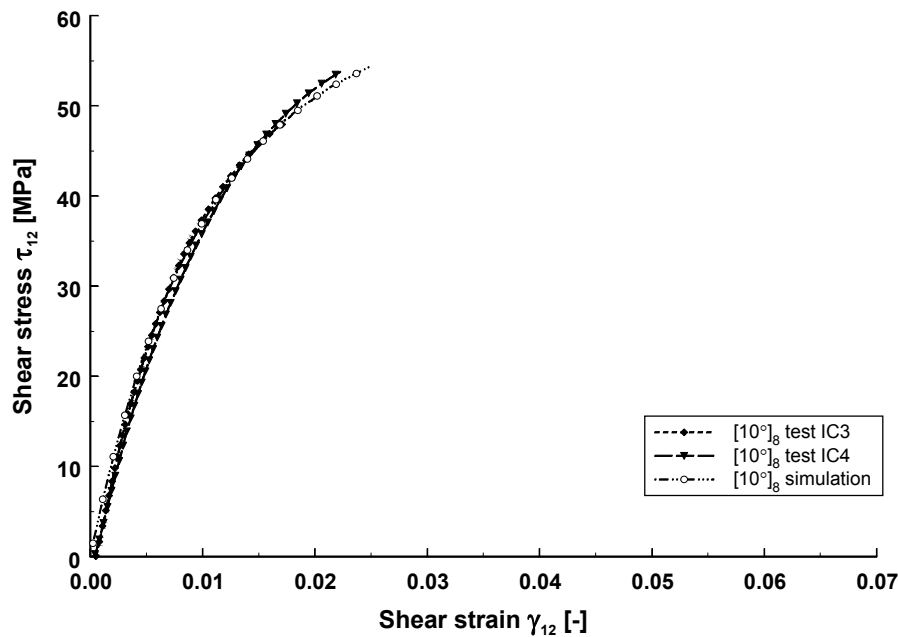


Figure 4 Experimental and simulated shear stress-strain curve for the static  $[10^\circ]_8$  tensile tests IC3 and IC4.

### 3. Finite element simulations

In this paragraph, the tensile tests on  $[+45^\circ/-45^\circ]_{2s}$  laminates and off-axis  $[10^\circ]_8$  composites are simulated with finite element software where the evolution laws for the shear damage  $D_{12}$  and the permanent shear strain  $\gamma_{12}^p$  have been implemented in the user material subroutine.

The commercial implicit finite element code SAMCEF<sup>TM</sup> was used. The results are first discussed for the tensile tests on  $[+45^\circ/-45^\circ]_{2s}$  laminates.

#### 3.1. $[+45^\circ/-45^\circ]_{2s}$ specimens

Figure 5 shows the finite element mesh for the  $[+45^\circ/-45^\circ]_{2s}$  specimen. The elements are isoparametric brick elements with second-degree interpolation. Each composite ply is modelled with one element through the thickness. The displacement is prescribed along the X-axis. As the damage model does not take into account time-dependent effects (strain-rate, visco-elasticity), the prescribed displacement  $u_x$  in the finite element simulations is assumed to increase linearly with some pseudo-time ranging from 0 to 1. Therefore, the time indicator for the finite element simulations has no relation with the time abscis from the experiments. Further, the prescribed displacement  $u_x$  in the simulations cannot be compared directly with the applied displacement in the experiments, because effects of slip in the grips are not accounted for in the simulations.

All the simulations have been done until the level of 7 % total shear strain  $\gamma_{12}$  was reached which corresponds with the ultimate measured value in the experimental tests. Simulations were done on a Sun Blade workstation and took about three days calculation time. Due to the highly nonlinear behaviour, the convergence rate was very slow.

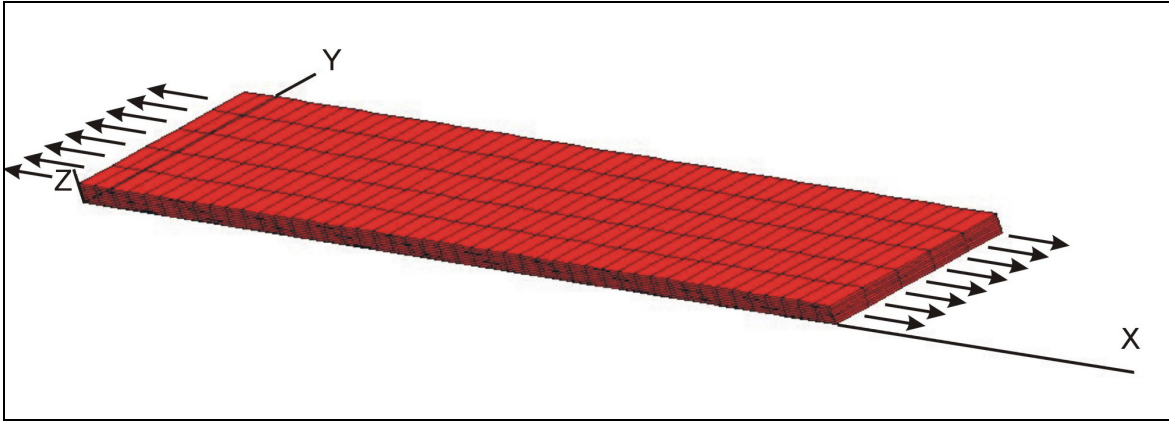


Figure 5 Finite element mesh for the  $[+45^{\circ}/-45^{\circ}]_{2s}$  specimen.

Figure 6 shows the calculated displacement contours at maximum displacement.

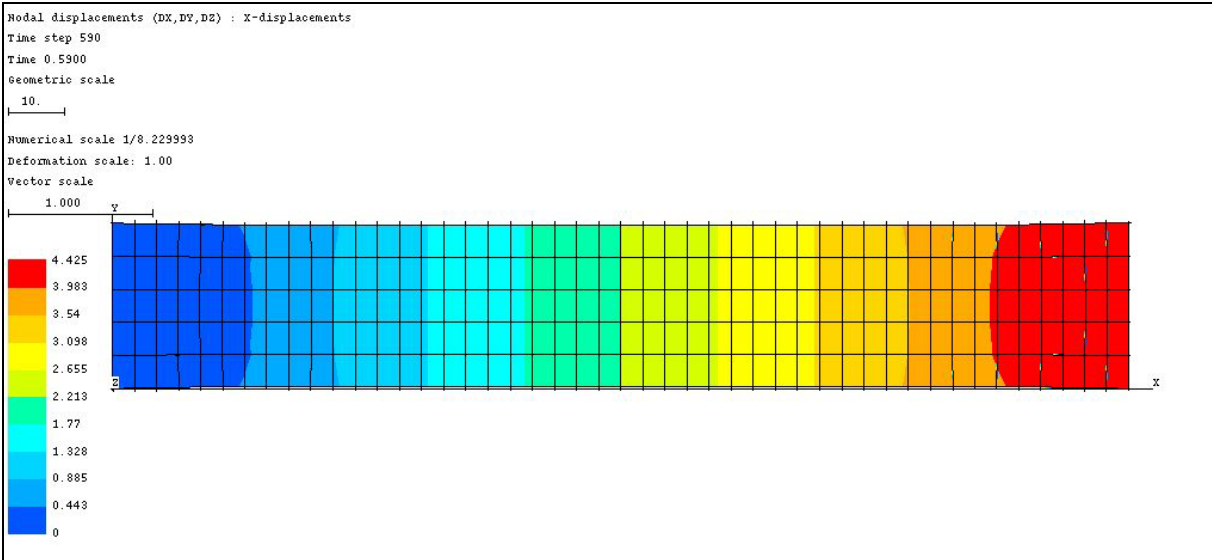
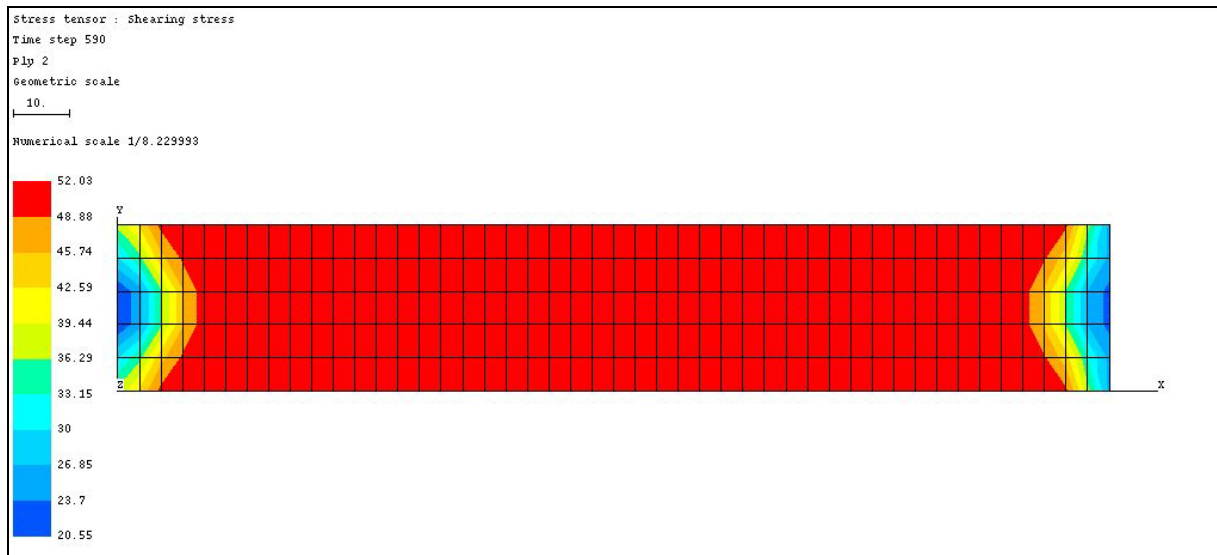


Figure 6 Simulated contours of displacement  $u_x$  for the  $[+45^{\circ}/-45^{\circ}]_{2s}$  specimen.

As can be seen from Figure 7, the simulated contours of the shear stress  $\tau_{12}$  show a constant value of 52.03 MPa for the shear stress in the whole specimen, apart from the areas close to the grips. The orientation of the fibres in the layer shown is  $-45^{\circ}$ .



**Figure 7** Simulated contours of shear stress  $\tau_{12}$  for the  $[+45^\circ/-45^\circ]_{2s}$  specimen.

The transverse stress  $\sigma_{22}$  reaches a value of about 30.0 MPa, but in the vicinity of the grips, stress concentrations do occur. The orientation of the fibres in the layer shown is  $-45^\circ$ .

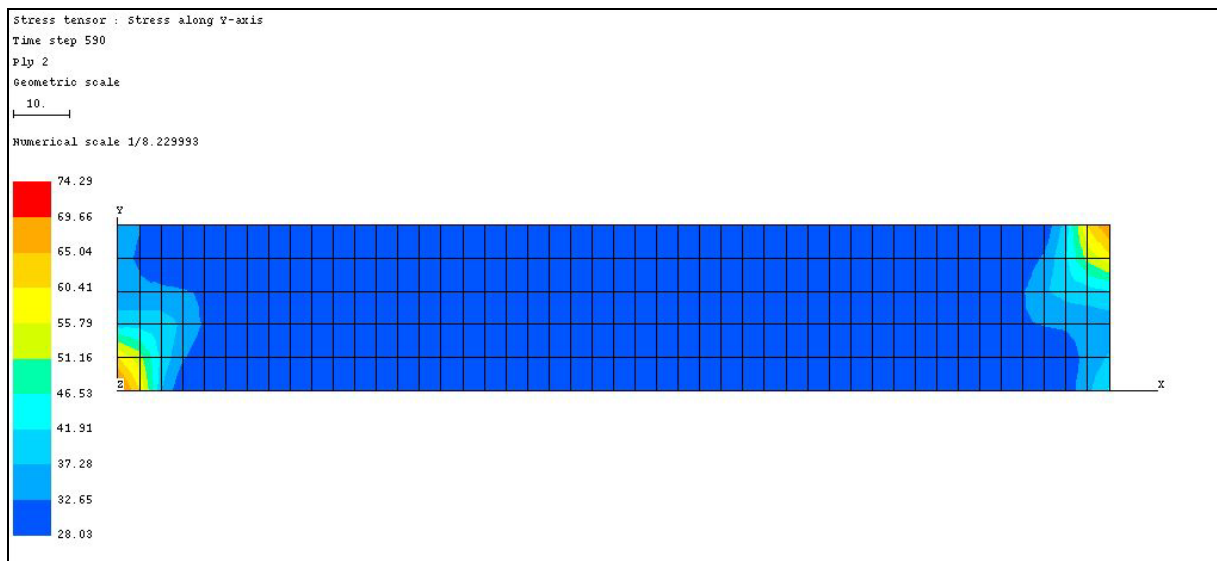


**Figure 8** Simulated contours of transverse stress  $\sigma_{22}$  for the  $[+45^\circ/-45^\circ]_{2s}$  specimen.

Finally Figure 9 shows the simulated time history of the inplane strains  $\epsilon_{11}$ ,  $\epsilon_{22}$  and  $\gamma_{12}$ . If this Figure is compared with the experimental results of Part I [1], Figure 5, the correspondence is very good.

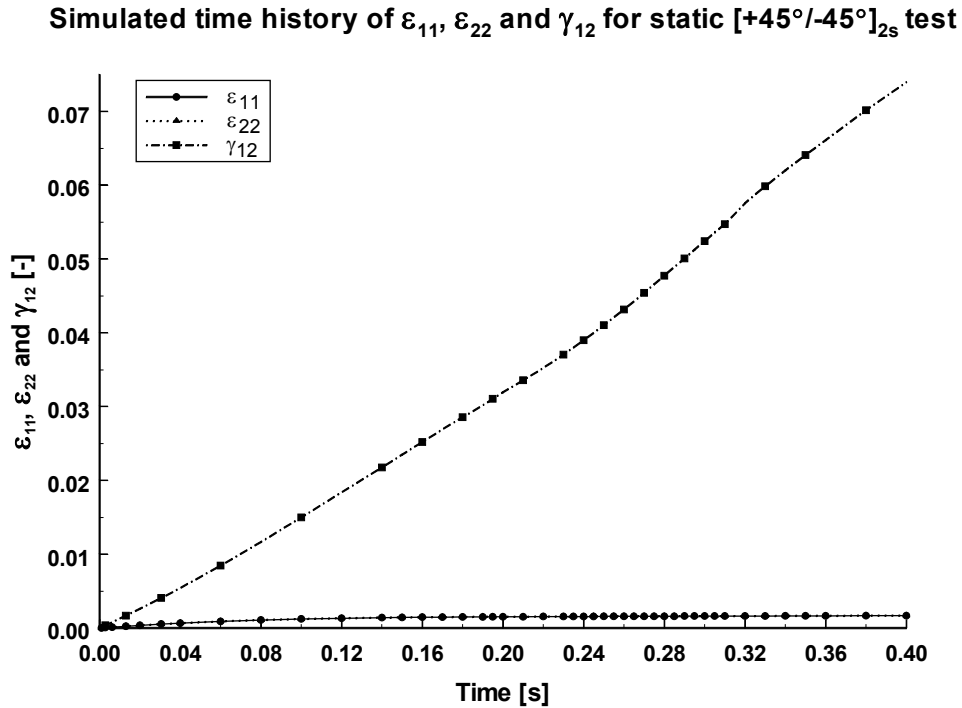
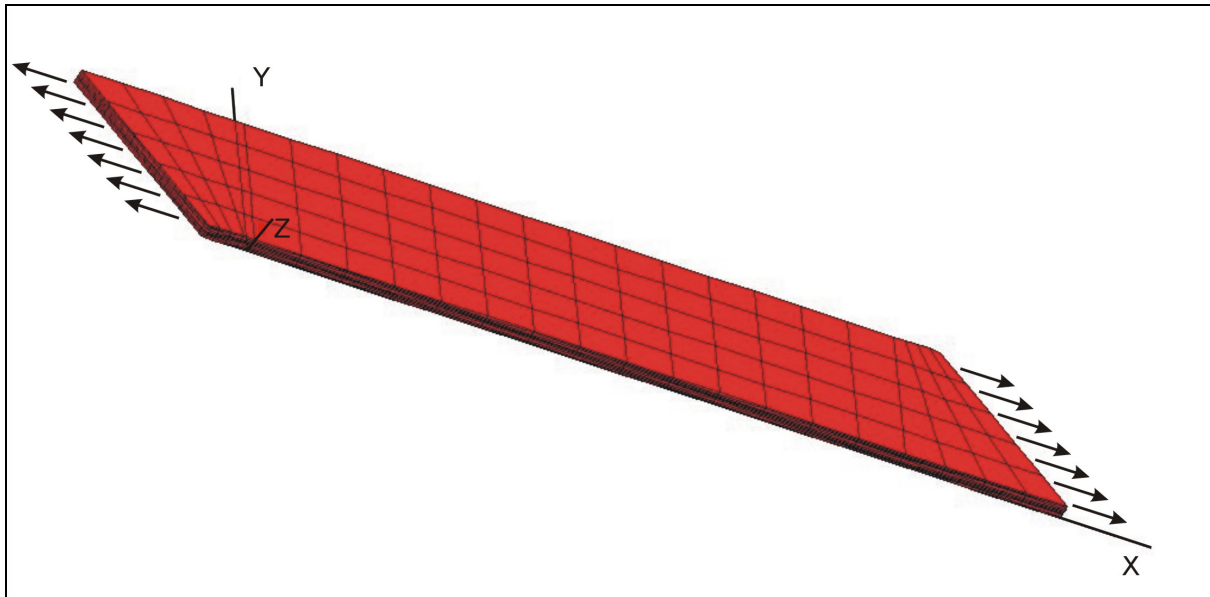


Figure 9 Simulated time history of the inplane strains  $\varepsilon_{11}$ ,  $\varepsilon_{22}$  and  $\gamma_{12}$  for the  $[+45^\circ/-45^\circ]_{2s}$  specimen.

### 3.2. $[10^\circ]_8$ specimens

Figure 10 shows the finite element mesh for the off-axis  $10^\circ$  specimens. Again, the elements are isoparametric brick elements with second-degree interpolation. Each composite ply is modelled with one element through the thickness. The displacement is prescribed along the X-axis.

The simulations have been done until the level of 1.7 % total shear strain  $\gamma_{12}$  was reached which corresponds with the ultimate measured value in the experimental test IC3.



**Figure 10** Finite element mesh for the  $[10^\circ]_8$  specimen.

Figure 11 shows the simulated displacement contours. As can be seen, the lines of constant displacement are no longer parallel with the oblique end tabs. Could it be that the calculated oblique angle  $\phi$  of  $54^\circ$  was not correct ?

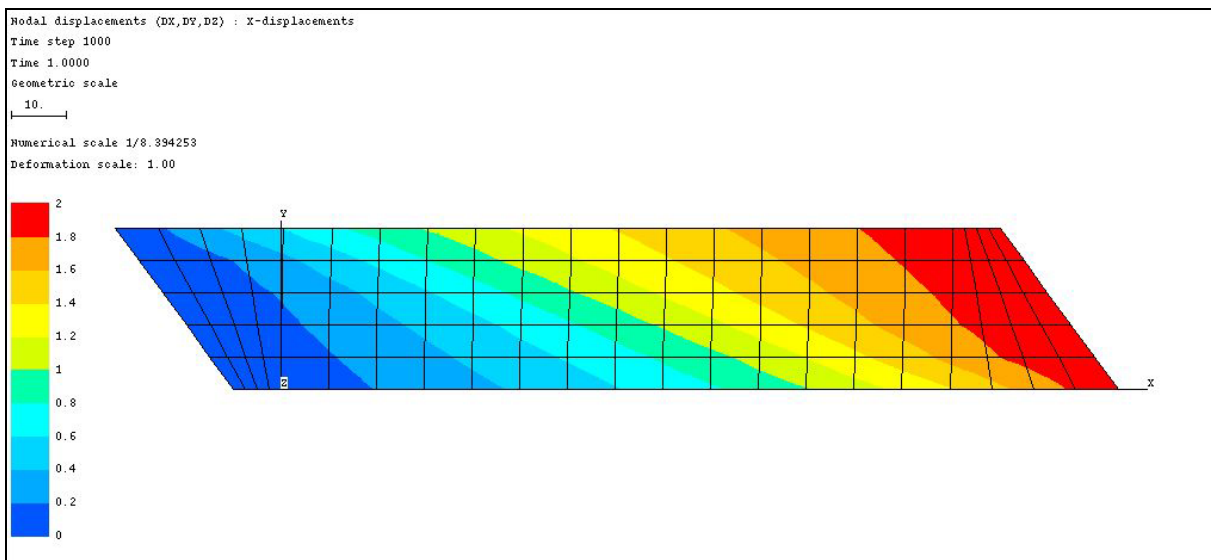


**Figure 11** Simulated contours of displacement  $u_x$  for the  $[10^\circ]_8$  specimen.

Therefore the simulation was done again, with the same mesh but without the material nonlinearities, so with a linear elastic material model. The calculated displacement contours are shown in Figure 12. In this case, the contours are parallel with the end tabs.

The disagreement is explained as follows: in the formula for calculation of the oblique angle  $\phi$ , the value of the virgin shear modulus  $G_{12}^0$  of the  $[10^\circ]_8$  off-axis specimens is needed. Due to the introduction of the shear damage  $D_{12}$ , the shear modulus  $G_{12}$  is decreasing and the iso-displacement lines do not longer follow the angle of the end tabs. Of course, this phenomenon cannot be avoided in the experimental tests.

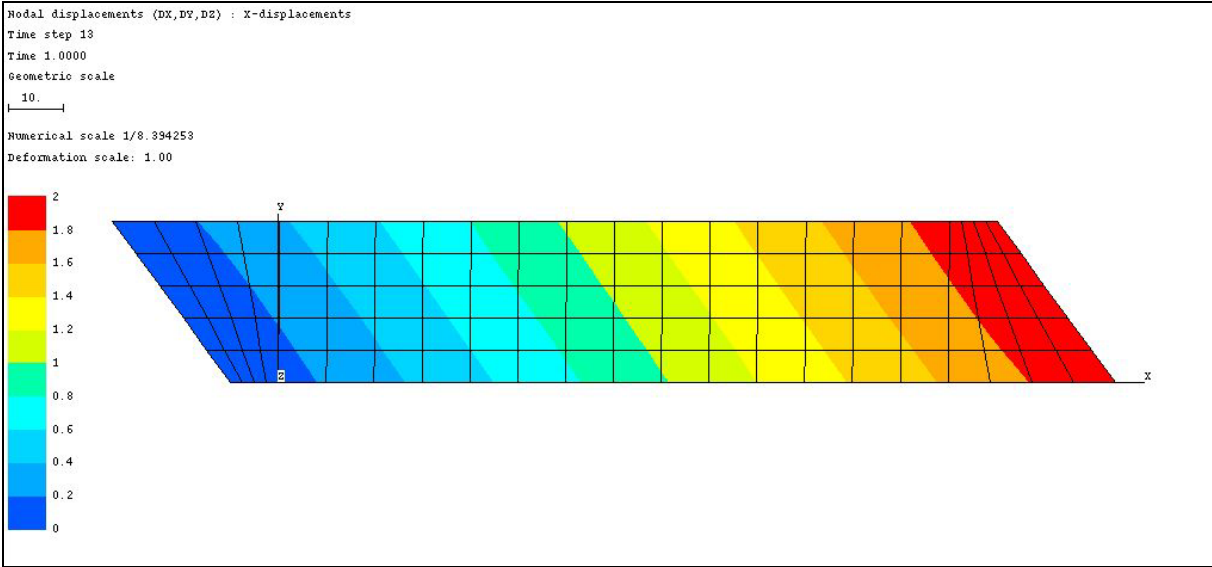


Figure 12 Simulated contours of displacement  $u_x$  for the  $[10^\circ]_8$  specimen without material nonlinearity.

Figure 13 shows the simulated contours of shear stress  $\tau_{12}$  at maximum displacement. Comparison with the picture of the failed specimens in Figure 14 shows a good agreement between the predicted failure site and the experimentally observed failure pattern.

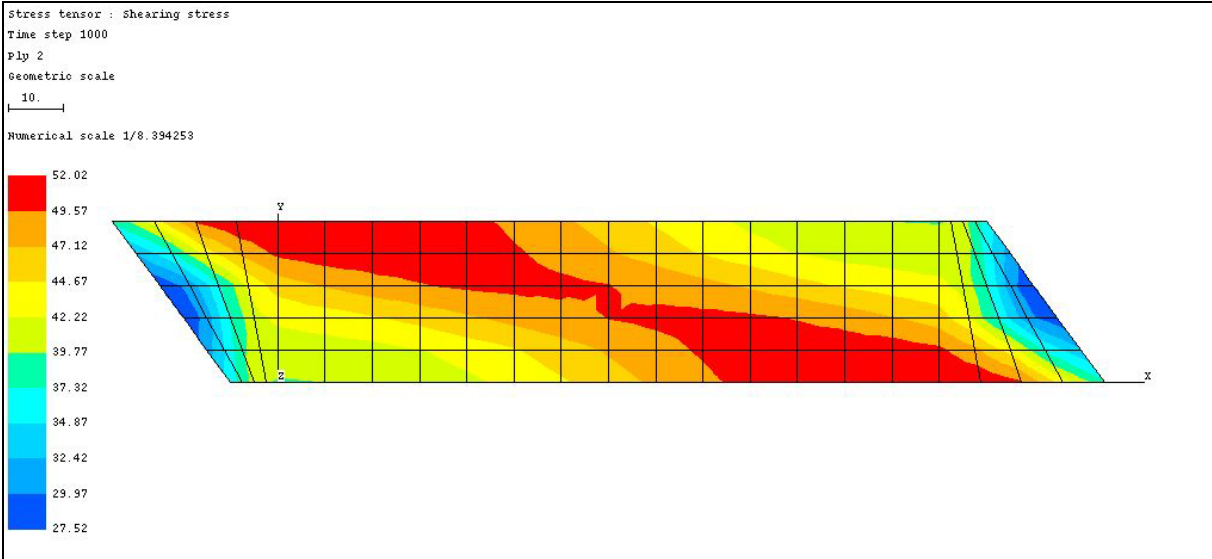


Figure 13 Simulated contours of shear stress  $\tau_{12}$  for the  $[10^\circ]_8$  specimen.

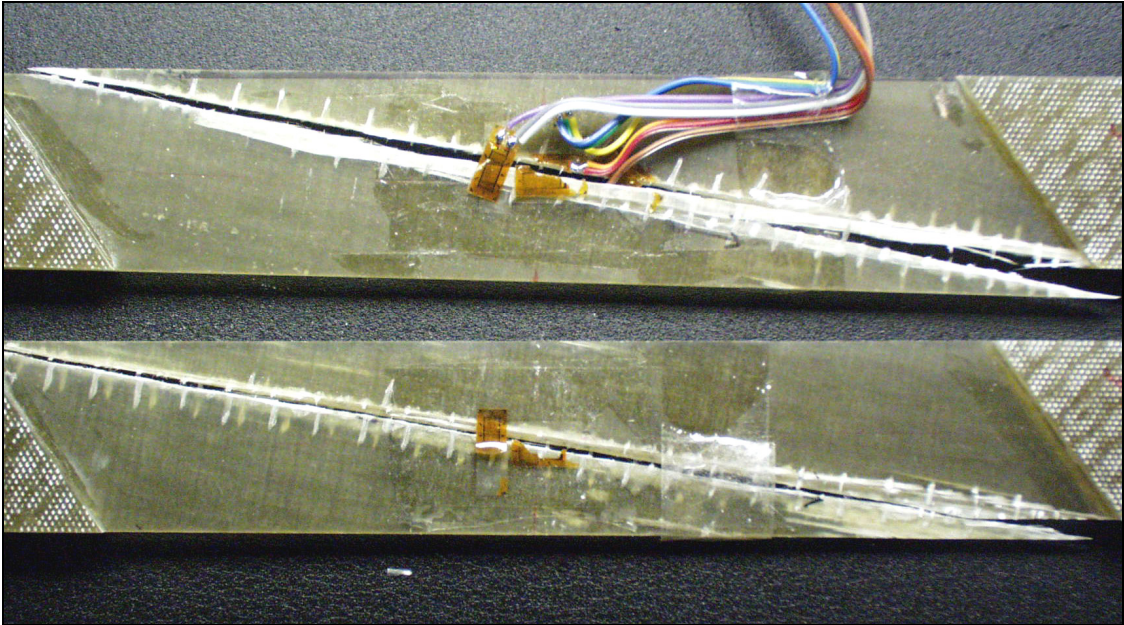


Figure 14 Experimentally observed failure pattern for the  $[10^\circ]_8$  specimens.

The value of the transverse stress  $\sigma_{22}$  reaches a value of about 8 MPa, but in the vicinity of the grips, much larger stresses do occur.

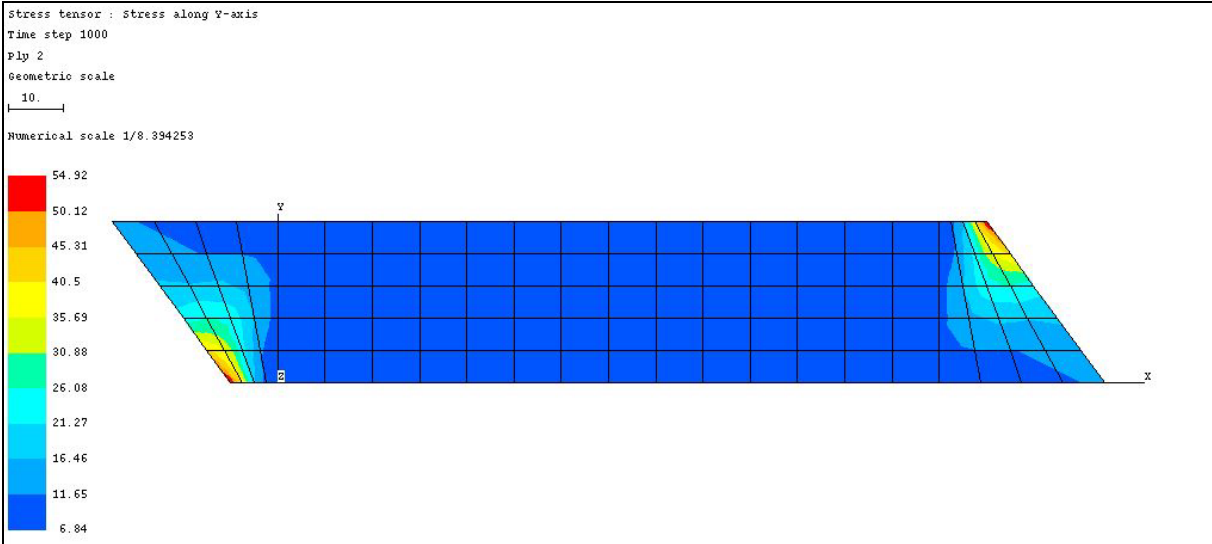


Figure 15 Simulated contours of transverse stress  $\sigma_{22}$  for the  $[10^\circ]_8$  specimen.

It was already observed from the experimental results in Part I [1] that the measured strain  $\epsilon_{22}$  is compressive, while the resulting stress  $\sigma_{22}$  is tensile. This is confirmed by the finite element results. The strain  $\epsilon_{22}$  is indeed compressive in the midsection of the specimen, as can be seen from Figure 16.



Figure 16 Simulated contours of transverse strain  $\epsilon_{22}$  for the  $[10^\circ]_8$  specimen.

Finally, Figure 17 shows the simulated time history of the strains  $\epsilon_{11}$ ,  $\epsilon_{22}$  and  $\gamma_{12}$ . If this Figure is compared with the experimental results of Part I [1], Figure 9, the correspondence is again very good.

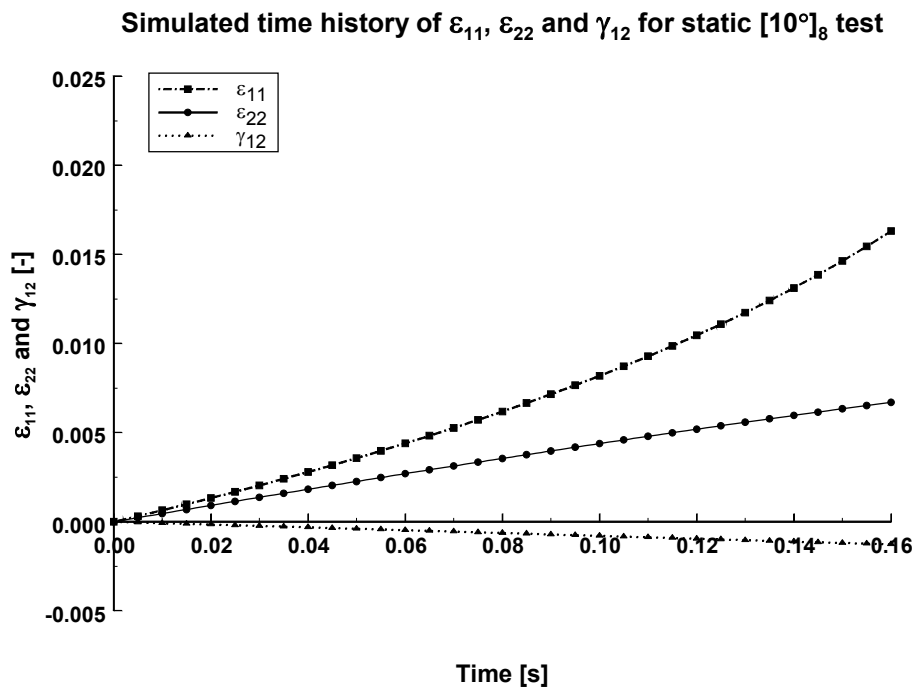
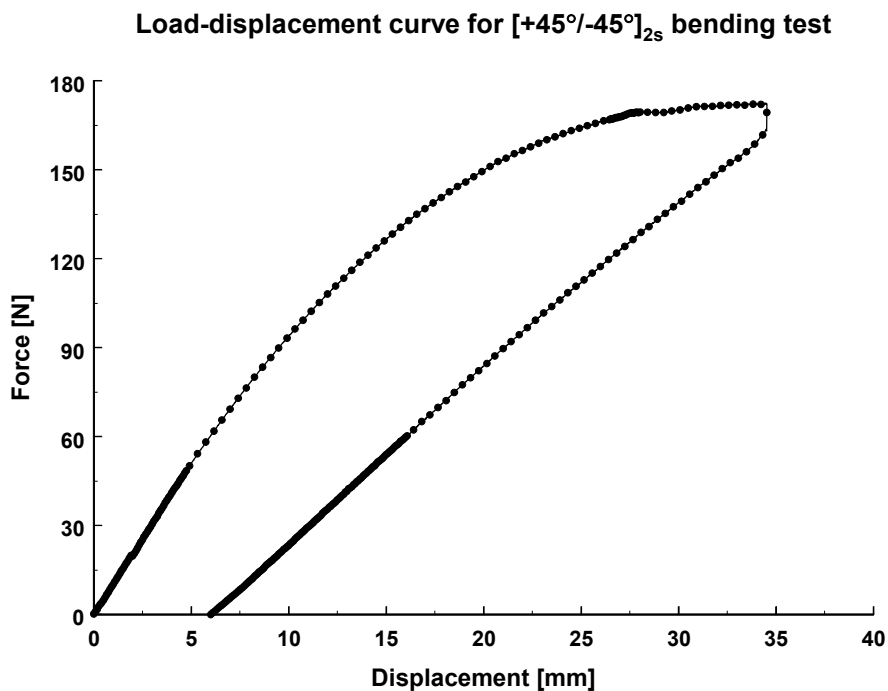


**Figure 17** Simulated time history of the inplane strains  $\epsilon_{11}$ ,  $\epsilon_{22}$  and  $\gamma_{12}$  for the  $[10^\circ]_8$  specimen.

#### 4. Validation

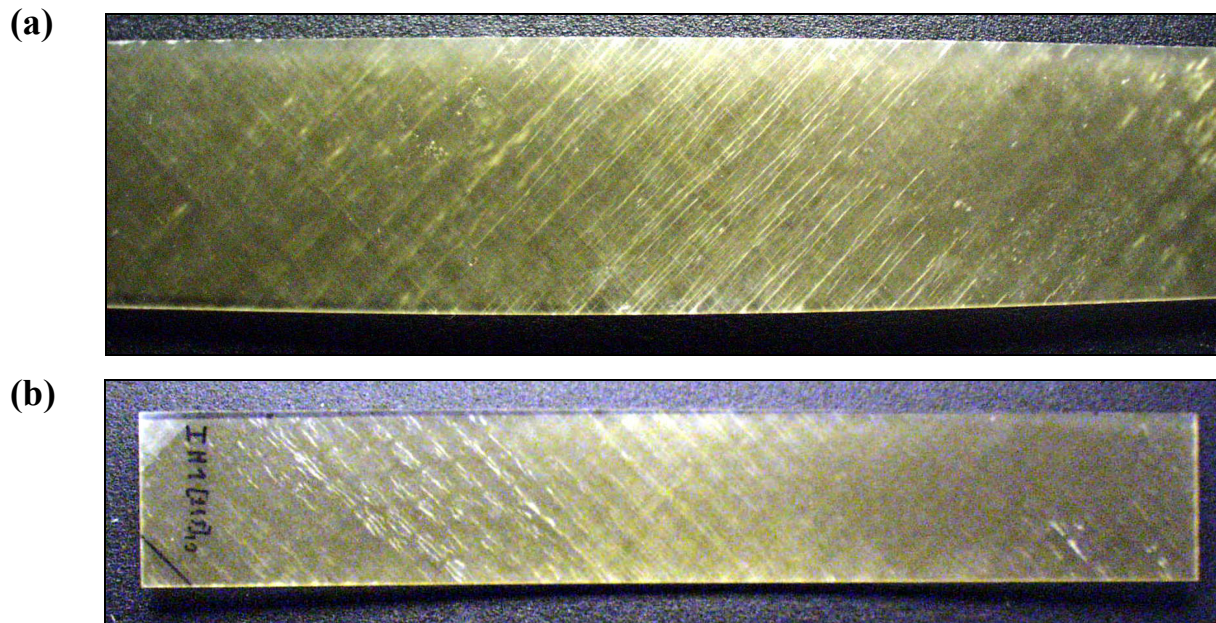
Although the material model for the shear stress-strain response of glass/epoxy laminates has been derived on the exclusive basis of *uni-axial tensile tests*, the quality of the model can be assessed further by applying the model to a bending test of a  $[+45^\circ/-45^\circ]_{2s}$  laminate.

Figure 18 shows the experimental load-displacement curve for a three-point bending test on the  $[+45^\circ/-45^\circ]_{2s}$  laminate. The test was displacement-controlled with a speed of 2 mm/min and the test was stopped at a maximum midspan deflection of 34.54 mm for a total span of 170 mm. Again, the response is highly nonlinear, with a considerable permanent deformation after unloading.



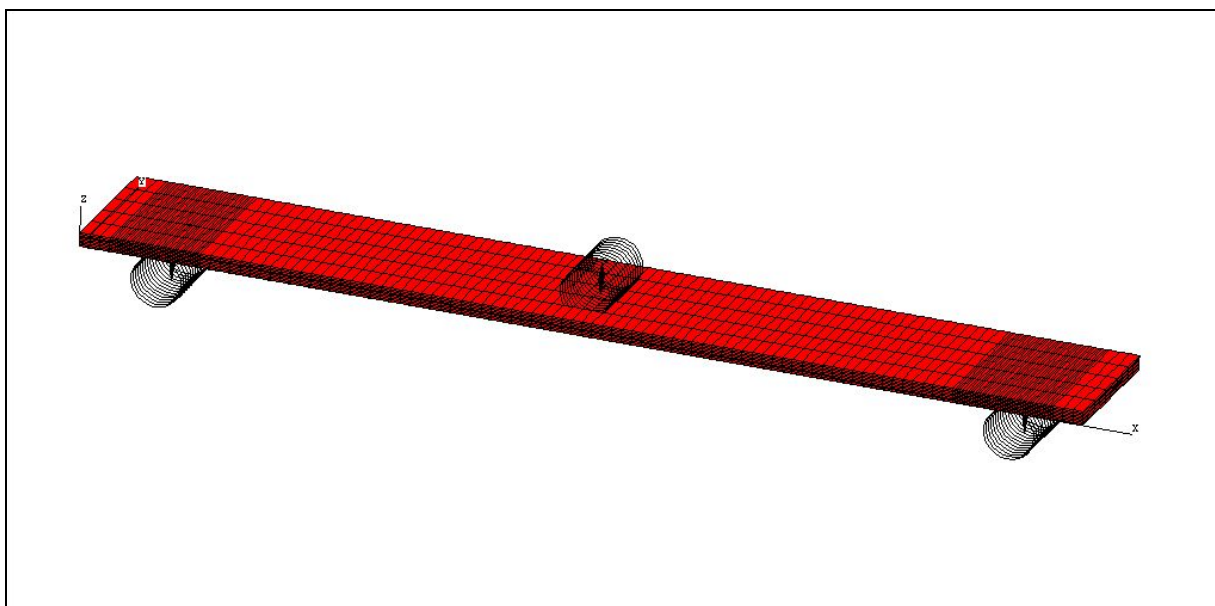
**Figure 18** Force-displacement curve for the three-point bending test of the  $[+45^\circ/-45^\circ]_{2s}$  specimen.

Figure 19 shows the corresponding damage patterns on the (a) tensile surface and (b) compressive surface of the  $[+45^\circ/-45^\circ]_{2s}$  laminate after unloading. First of all, it is important to mention that the test was stopped before final fracture occurred. The tensile surface shows a shear damage pattern that is very comparable with the one observed with the uni-axial tensile tests. The compressive surface, where  $\epsilon_{11}$  is negative, shows a less pronounced damage pattern, although there are white striations under  $-45^\circ$  in the area at the left and in the lower right corner.



**Figure 19** Damage patterns on the (a) tensile surface and (b) compressive surface of the  $[+45^\circ/-45^\circ]_{2s}$  specimen after unloading from the three-point bending test.

Figure 20 shows the corresponding finite element mesh. Two supports left and right and one load striking edge at midspan have been modelled as rigid body cylinders. The composite specimen has been modelled with isoparametric brick elements with second-degree interpolation. Contact conditions were defined between the two lower end-supports and the surface of the specimen and a very fine mesh was needed there to assure the convergence. Geometrical nonlinearities were accounted for and the complete loading-unloading path was simulated.

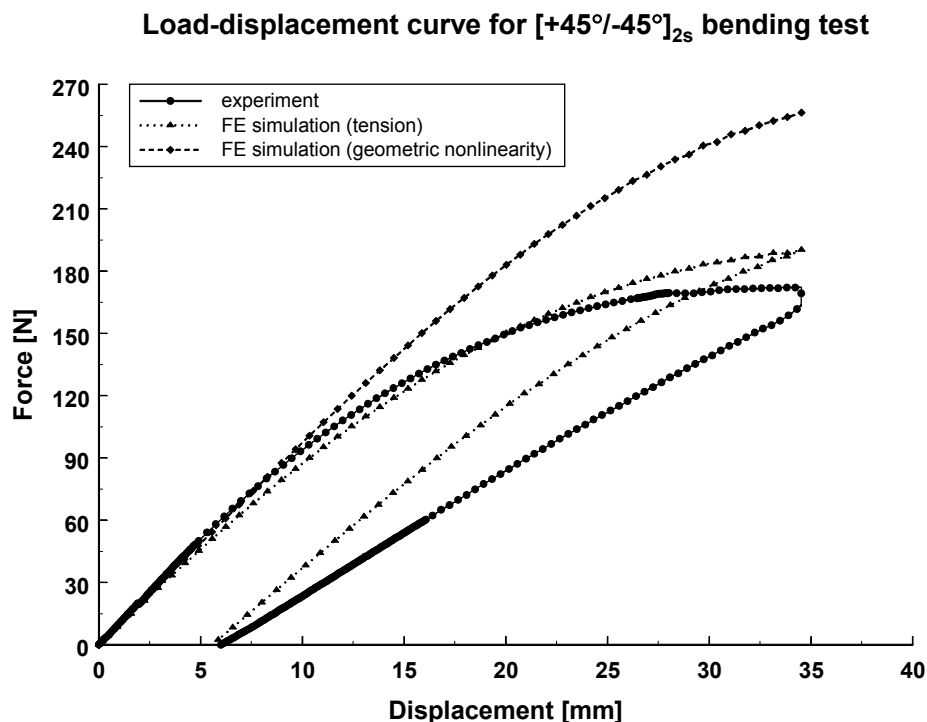


**Figure 20** Finite element mesh for the three-point bending test of the  $[+45^\circ/-45^\circ]_{2s}$  specimen.

The material model for the shear response of the  $[+45^\circ/-45^\circ]_{2s}$  laminate was developed from tensile tests with  $\varepsilon_{11}$  and  $\varepsilon_{22}$  being small, but yet always positive. Here, shear strain is combined with either positive or negative normal strains, depending on the position with respect to the neutral axis, and this affects the damage pattern, as could be seen from Figure 19.

The first simulation has been done with the developed material model applied only to the part where  $\varepsilon_{11}$  is positive, and including the geometrical nonlinearities. Figure 21 shows the simulated force-displacement curve for the complete loading-unloading cycle. To assess the effect of the material nonlinearities, the same simulation has been done without material nonlinearities, but of course with geometrical nonlinearities accounted for.

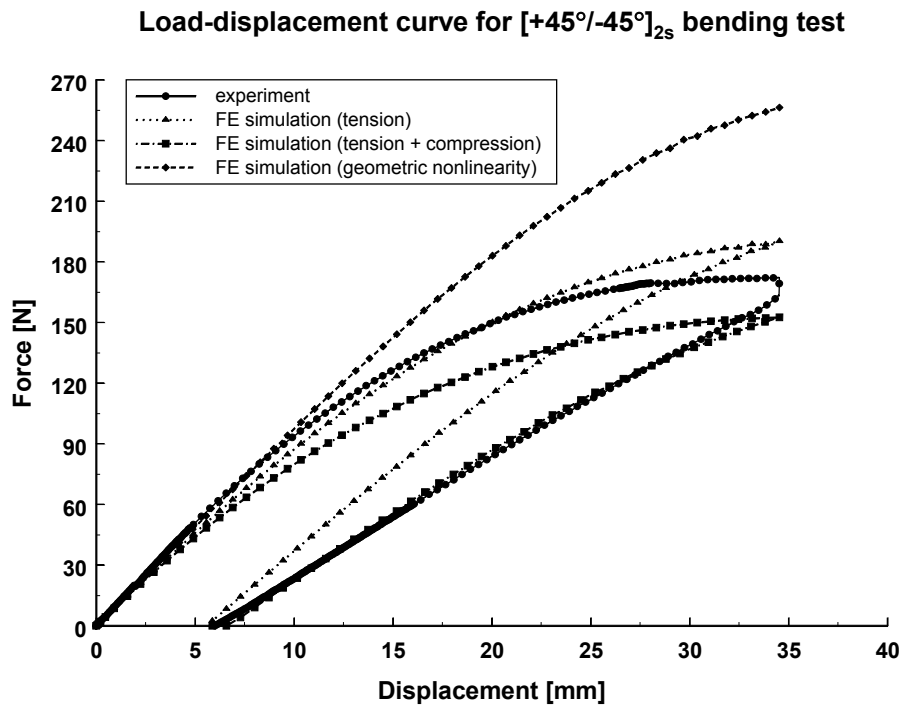
It can be clearly seen that the finite element simulation with material nonlinearities greatly improves the result, compared to the finite element simulation with only geometrical nonlinearities. Also the remaining permanent deflection is predicted very well. However, in the last part of the loading stage, the force is overestimated. This could be expected, because the nonlinear shear response has only been taken into account for the part where  $\varepsilon_{11}$  is positive, although Figure 19 clearly showed that damage developed as well at the upper surface. As the permanent deflection can be largely attributed to the permanent shear strain, that correspondence is much better.



**Figure 21** Experimental and simulated load-displacement curve for the three-point bending test of the  $[+45^\circ/-45^\circ]_{2s}$  specimen.

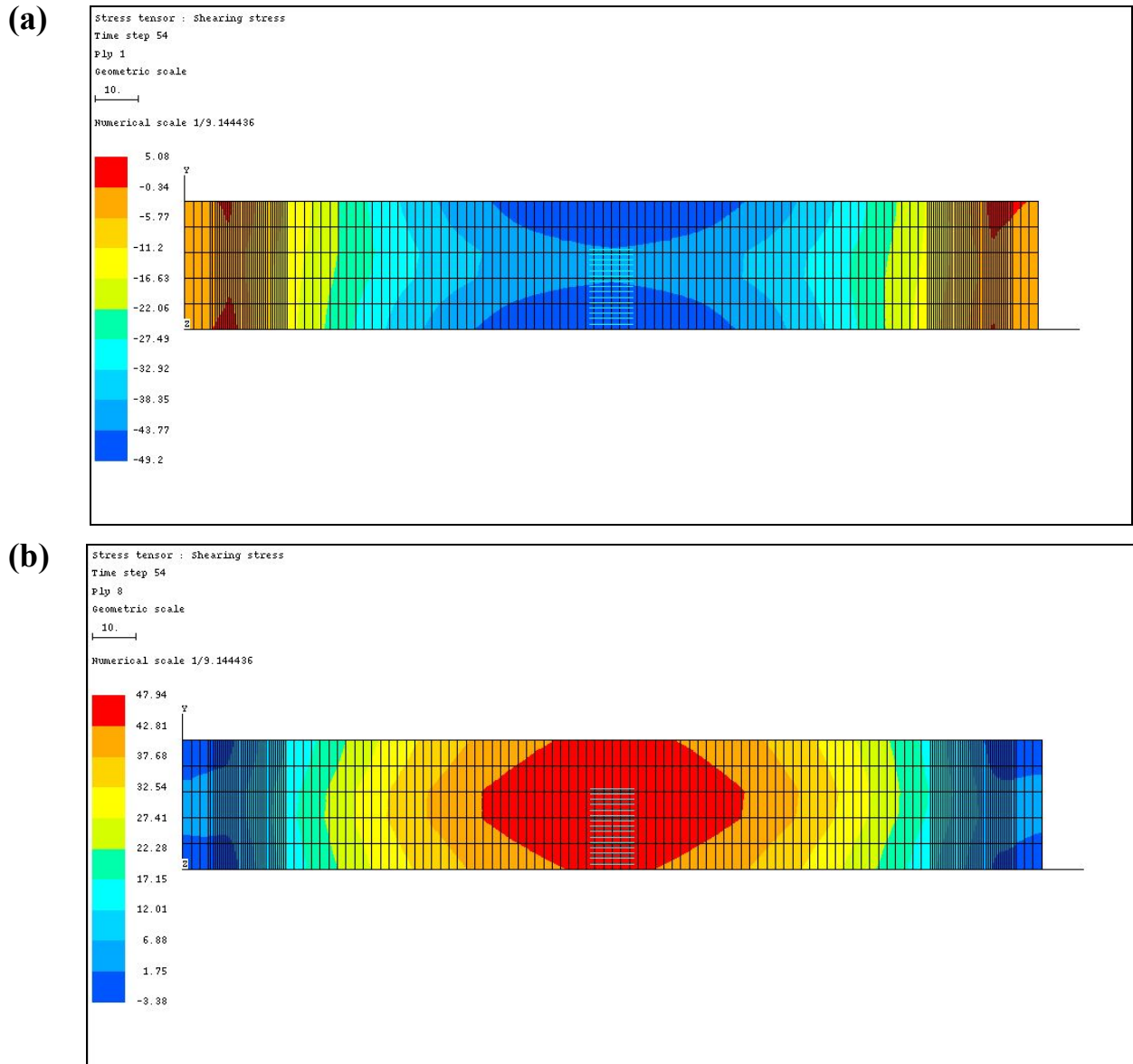
Therefore, the second simulation applies the material model for the shear response to the whole specimen, also to the part where  $\varepsilon_{11}$  is negative. The corresponding results are shown in

Figure 22. The results are very similar with the ones in Figure 21, but now the force is underestimated in the last part of the loading stage.



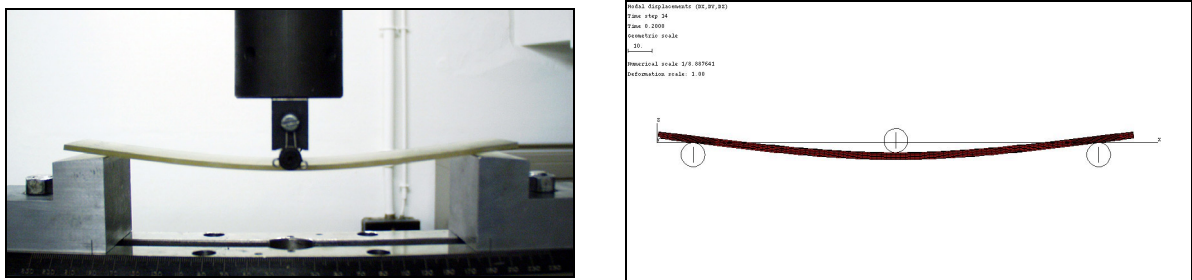
**Figure 22** Experimental and simulated load-displacement curve for the three-point bending test of the  $[+45^\circ/-45^\circ]_{2s}$  specimen.

Figure 23 shows the simulated contours of the shear stress  $\tau_{12}$  at the maximum deflection of 34.54 mm for (a) the tensile surface and (b) the compressive surface. The fibre direction in both layers is  $+45^\circ$ .



**Figure 23** Simulated contours of the shear stress  $\tau_{12}$  on the (a) tensile surface and (b) compressive surface of the  $[+45^\circ/-45^\circ]_{2s}$  specimen at maximum deflection.

Figure 24 shows the correspondence between the pictures taken from the experimental test, and the finite element simulation, for four different stages of loading.



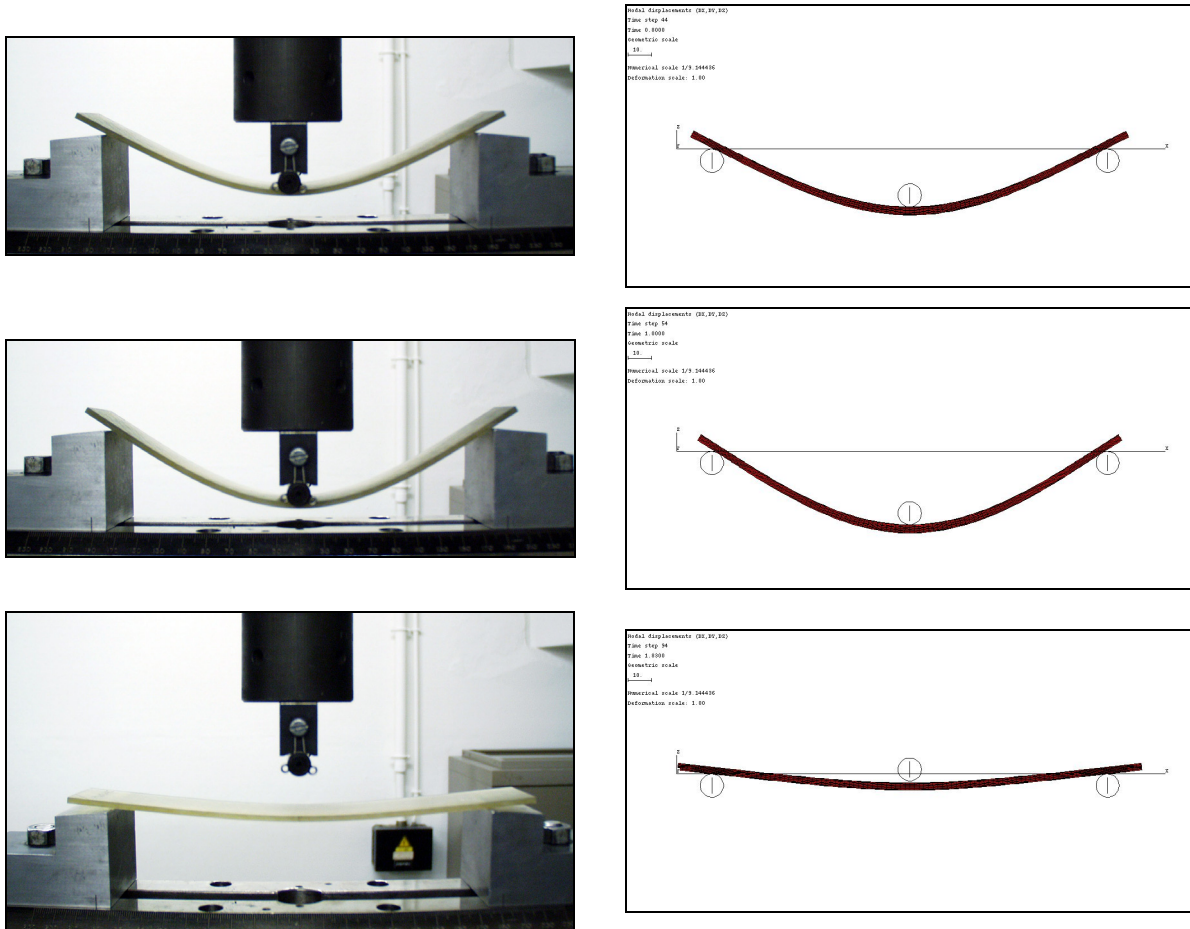


**Figure 24** Experimental and simulated bending profile for the three-point bending test of the  $[+45^\circ/-45^\circ]_{2s}$  specimen at four different stages: (i) 7.08 mm, (ii) 27.87 mm, (iii) 34.54 mm (maximum displacement, and (iv) after reloading.

It is clear that the two finite element simulations determine the upper and lower bound of the experimental response, but none of them accurately predicts the nonlinear part of the force-displacement curve. The most important reason for this is the combined stress state in the three-point bending test. The uni-axial tensile test of the  $\pm 45^\circ$  composite laminate is based on the assumption that the stresses  $\sigma_{11}$  and  $\sigma_{22}$  remain very small. This is not the case anymore in the three-point bending test. Figure 25 shows the simulated contours of the stresses (a)  $\sigma_{11}$  and (b)  $\sigma_{22}$  at the maximum deflection of 34.54 mm for the tensile surface. The fibre direction in both layers is  $+45^\circ$ .

It is clear that especially the transverse stress  $\sigma_{22}$  reaches very high values and that its different sign below and above the neutral fibre (tensile or compressive) must affect the shear damage evolution in the ply.

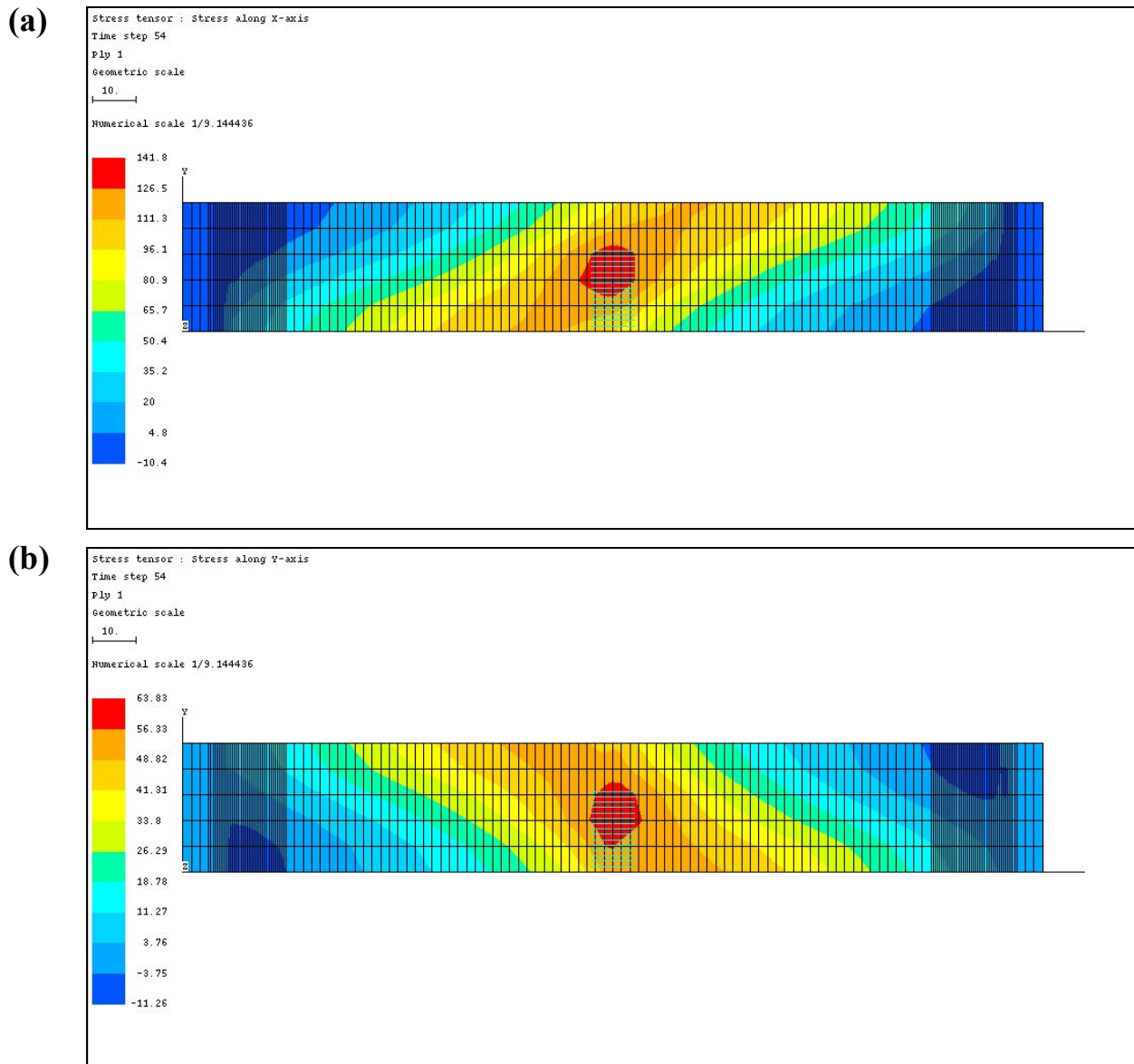


**Figure 25 Simulated contours of the stresses (a)  $\sigma_{11}$  and (b)  $\sigma_{22}$  at the tensile surface of the  $[+45^\circ/-45^\circ]_{2s}$  specimen at maximum deflection.**

## 5. Conclusions

The nonlinear shear response of long glass fibre-reinforced epoxy composites has been modelled. A material model was developed with two state variables: the shear damage  $D_{12}$  and the permanent shear strain  $\gamma_{12}^p$ . Their evolution laws were derived from the experimental data.

The finite element simulations of the tensile tests on  $[+45^\circ/-45^\circ]_{2s}$  laminates and off-axis  $[10^\circ]_8$  composites show good agreement with the measured strain histories and the observed failure patterns. A final validation of the model for a three-point bending test on a  $[+45^\circ/-45^\circ]_{2s}$  laminate shows that the shear damage and permanent shear strain can be simulated satisfactorily, but that the effect of the higher normal stresses  $\sigma_{11}$  and  $\sigma_{22}$  cannot be neglected. Additional damage laws for the transverse stiffness should be developed for that purpose.

## Acknowledgements

The author W. Van Paepegem gratefully acknowledges his finance through a grant of the Fund for Scientific Research – Flanders (F.W.O.).

## References

[1]	Van Paepegem, W., De Baere, I. and Degrieck, J. (2005). Modelling the nonlinear shear stress-strain response of glass fibre-reinforced composites. Part I: Experimental results. <i>Composites Science and Technology</i> , xx(x), xx-xx.
[2]	Yuan, F.G., Pagano, N.J. and Cai, X. (1997). Elastic moduli of brittle matrix composites with interfacial debonding. <i>International Journal of Solids and Structures</i> , 34(2), 177-201.
[3]	Aboudi, J. (1990). The nonlinear behaviour of unidirectional and laminated composites - A micromechanical approach. <i>Journal of Reinforced Plastics and Composites</i> , 9, 13-32.
[4]	Aboudi, J. (1987). Damage in composites - Modeling of imperfect bonding. <i>Composites Science and Technology</i> , 28, 103-128.
[5]	Ladeveze, P. and Le Dantec, E. (1992). Damage modelling of the elementary ply for laminated composites. <i>Composites Science and Technology</i> , 43, 257-267.
[6]	Payan, J. and Hochard, C. (2002). Damage modelling of laminated carbon/epoxy composites under static and fatigue loadings. <i>International Journal of Fatigue</i> , 24, 299-306.
[7]	Lafarie-Frenot, M.C. and Touchard, F. (1994). Comparative in-plane shear behaviour of long-carbon-fibre composites with thermoset or thermoplastic matrix. <i>Composites Science and Technology</i> , 52, 417-425.